Nonlinear Dynamics of Ultrashort Long-Range Surface Plasmon Polariton Pulses in Gold Strip Waveguides

Lysenko, Oleg; Bache, Morten; Olivier, Nicolas; Zayats, Anatoly V.; Lavrinenko, Andrei

Published in:
ACS Photonics

Link to article, DOI:
10.1021/acsphotonics.6b00509

Publication date:
2016

Document Version
Peer reviewed version

Nonlinear Dynamics of Ultrashort Long-Range Surface Plasmon Polariton Pulses in Gold Strip Waveguides

Oleg Lysenko,[*,†,§] *Morten Bache,*[†,§] *Nicolas Olivier,*[‡,∥] *Anatoly V. Zayats,*[‡] *and Andrei Lavrinenko*[†]

[†]Department of Photonics Engineering, Technical University of Denmark, Oersteds Plads, Building 345 V, Kongens Lyngby 2800, Denmark

[‡]Department of Physics, King's College London, Strand, London WC2R 2LS, UK

KEYWORDS: plasmonics, nonlinear optics, ultrafast nonlinearity

ABSTRACT: We study experimentally and theoretically nonlinear propagation of ultrashort long-range surface plasmon polaritons in gold strip waveguides. The nonlinear absorption of the plasmonic modes in the waveguides is measured with femtosecond pulses revealing a strong dependence of the third-order nonlinear susceptibility of the gold core on the pulse duration and layer thickness. A comprehensive model for the pulse duration dependence of the third-order nonlinear susceptibility is developed on the basis of the nonlinear Schrödinger equation for plasmonic mode propagation in the waveguides. The model accounts for the intrinsic delayed (noninstantaneous) nonlinearity of free electrons of gold as well as the thickness of the gold film, and is experimentally verified. The obtained results are important for the development of active plasmonic and nanophotonic components.

Plasmonic nanostructures represent a unique platform for many linear and nonlinear optical applications.[1] A great variety of plasmonic waveguides for integrated optics,[2,3] nanofocusing,[4,5] sensing,[6,7] lasing and amplification of light[8,9] has been proposed. In particular, special attention has recently been paid to the nonlinear optical properties of plasmonic waveguides, hybrid plasmonic waveguides, and other elements important for future nanophotonic communication approaches.[10–12] Bulk metals, thin metal layers, and plasmonic metamaterials have been investigated in the nonlinear regime.[13–15]

The nonlinear propagation of surface plasmon polaritons (SPPs) in plasmonic waveguides can be studied in terms of either the second-order nonlinearity,[16,17] or the third-order nonlinearity.[18,19] The latter is particularly important because it is present in all materials. In metals, it mainly arises due to hot-electron contributions from changes of the intrinsic electronic temperature after absorption of the incident light. Typically, the electron relaxation time in noble metals is on the few-picosecond scale,[18,19] implying that their nonlinear susceptibility can depend on the laser pulse duration if it is shorter than or comparable with the electron relaxation time.[20] The majority of the experimental data on the third-order nonlinear susceptibility of gold were collected near the interband transitions in a wavelength range of 532-630 nm for pulse durations between 100 fs and 1 ns.[20] Most results were obtained with the z-scan method, reporting very high values of the third-order susceptibility in the range of 10^{-16}-10^{-15} m^2/V^2.[21–24] However, the linear propagation losses of SPPs in Au-based waveguides, which are also related to the same interband transitions, are very high (~30-40 dB/mm) in this wavelength range.[25]

On the other hand, nanophotonic and plasmonic devices are extensively exploited in the infrared (IR) wavelength range.[2,3] The propagation losses of long-range SPPs (LRSPPs) in Au-based waveguides can be ~2-5 dB/mm at the telecommunication wavelengths.[25] Meanwhile, the third-

order susceptibility of gold, $\chi^{(3)}_{\mathrm{Au}}$, in the IR wavelength range arises mainly from the intraband electron transitions and is much smaller than in the visible range.[18,19] Therefore, a conventional z-scan method may not be sensitive enough for nonlinear measurements in ultrathin gold layers. Nevertheless, the third-order nonlinearities of gold can be large enough to affect the signal propagation in a LRSPP waveguide due to the field localization near the metal interfaces and long propagation distance L_{SPP}.[26,27]

The third-order susceptibility of a gold film, which affects transmission (reflection) of light through (from) a film as well as propagation of plasmonic modes on the film interfaces is known to depend on both the pulse duration and thickness of the film.[20] The goal of this paper is to quantify such dependences in experiment and theory on nonlinear propagation of the LRSPP modes in Au strip waveguides. The nonlinear propagation is conditioned by the third-order susceptibility of gold,[18,19] and we use the nonlinear Schrödinger equation[28] for LRSPPs to study their propagation evolution. We measure the nonlinear absorption of the LRSPP mode in gold strip waveguides and present new experimental data on the imaginary part of the third-order susceptibility of gold for 200 fs pulses at a wavelength of 1030 nm. Since the same plasmonic waveguides were previously characterized with 3 ps pulses at a wavelength of 1064 nm,[26] the data can be directly compared to obtain an experimental dependence of the third-order susceptibility of gold on both the gold layer thickness and light pulse duration in the femtosecond-picosecond range. The obtained dependences confirm a significant increase in the third-order susceptibility for picosecond pulses over femtosecond ones due to better temporal overlap of longer pulses with the transient profile of the excited electron gas.[18,19] The data confirm that the ultrafast intrinsic "delayed" (i.e. noninstantaneous) temporal response function of free electrons in gold[18,19] is instrumental in modeling of the ultrashort LRSPP propagation

with a nonlinear Schrödinger equation, with the continuous wave (cw) value of the third-order susceptibility being a single free parameter. We also report thickness scaling laws describing the enhanced nonlinearity in gold strip waveguides.

The LRSPP waveguides studied here were fabricated using procedure described earlier [26]. A silicon wafer with a thick (approximately 6.5 μm) layer of silicon dioxide on top was used as a substrate. Standard ultraviolet lithography was applied to pattern a photoresist layer. A metal layer and adhesion layers were then deposited by sputtering. After removing the photoresist layer, the waveguides profile and metal layer roughness were measured with an atomic force microscope. The root mean square value for the roughness of the deposited metal layers is 0.67 nm. The metal layers are continuous that was also verified by using a scanning electron microscope. Finally, a cladding layer of silicon dioxide (approximately 5.5 μm) was deposited on top using a standard plasma-enhanced chemical vapor deposition method. The final waveguides consist of a thin gold layer with thickness t_{Au} = 22, 27 and 35 nm, sandwiched between 26 nm- thick tantalum pentoxide adhesion layers, and silicon dioxide claddings (Figure 1a). The linear and nonlinear optical properties of tantalum pentoxide are well-known,[29,30] and its use provides smaller propagation losses in plasmonic waveguides than metallic adhesion materials, such as titanium.[31] This symmetric arrangement provides a substantialpropagation length of LRSPPs of about 0.3-0.5 mm at a wavelength of 1030 nm depending on the gold layer thickness t_{Au}.[27]

Femtosecond pulses of 200 fs duration at a wavelength of 1030 nm were used to excite LRSPPs (see Supporting Information for the experimental setup details). The linear propagation loss of the LRSPP mode in the waveguides increases by a factor of 2 as the gold layer thickness increases from 22 nm to 35 nm, similar to the previous measurements at 1064 nm.[26] At the same

time, the end-fire coupling loss per two (in- and out-coupling) facets of the waveguides changes insignificantly. The obtained values for the linear propagation loss per unit length α at 1030 nm are about 10% higher than the corresponding values at 1064 nm[26] as expected for the reduction of material (Ohmic) losses with the wavelength.[2,25,32] The values of the propagation loss α and coupling loss C are shown in the Supplementary Information, Table S1. Although the values of the coupling loss C for the free-space lens coupling are around 7 dB per two facets, i.e. approximately 3 dB higher than the corresponding values for the fiber coupling,[26] the free-space coupling method used here is preferred to exclude dispersion effects when operating with femtosecond pulses.[28]

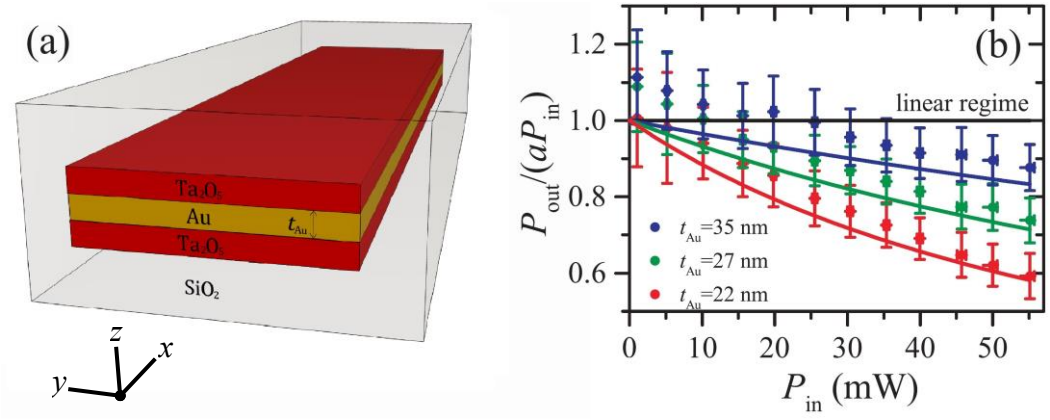

Figure 1. (a) Sketch of the LRSPP waveguide. (b) Nonlinear transmission dependences for 200 fs pulses at a wavelength of 1030 nm in the strip plasmonic waveguides with t_{Au} = 22, 27, and 35 nm.

The nonlinear propagation of the LRSPP mode in the waveguides was characterized by tuning the average input power P_{in} in the range 1-55 mW (as described in Supporting Information). The electron thermalization rate in gold[18,19] is much larger than the laser repetition rate used in the experiment (f_{rep} = 200 kHz), implying that each laser pulse interacts individually. The linear and

nonlinear losses of the LRSPP mode are modeled by the following equation:[27] $\partial_x P = -\alpha P - \beta P^2$, where β is the nonlinear two-photon absorption coefficient,[27,33] P is the instantaneous power, and x is the propagation coordinate. The solution to this equation can be expressed in terms of the normalized average power right after the waveguide for a Gaussian pulse as follows:[27] $P_{out}/(aP_{in}) = 1/[1+\beta L_{eff} P_{in} e^{-C/2}/(\sqrt{\pi}\tau_0 f_{rep})]$, where $L_{eff} = [1-\exp(-\alpha L)]/\alpha$ is the effective propagation length,[28] L is the physical length of the waveguide, τ_0 is the 1/e intensity half-width, and $a = \exp(-\alpha L - C)$ is the experimental coefficient that contains linear propagation loss α and coupling loss C. The nonlinear dependences of transmitted power P_{out} on input power P_{in} for the waveguides with the length L = 2 mm and the gold layer thickness t_{Au} = 22, 27, and 35 nm are shown in Figure 1b. The deviation from the horizontal line $P_{out} = aP_{in}$ is an indication of the two-photon absorption effect[27,33] represented by the nonlinear absorption coefficient β. The curves are fitted using β as the only free parameter and starting from unity at P_{in} = 0 for consistency of the linear and nonlinear regimes.

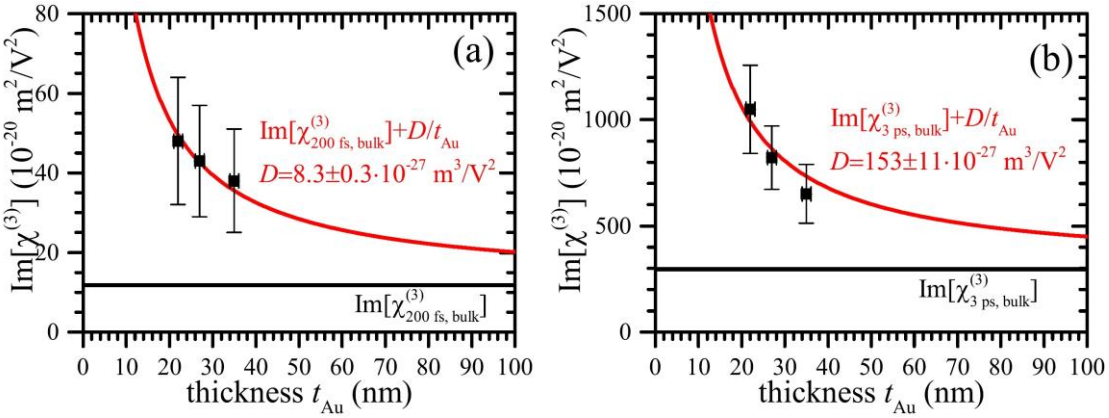

Figure 2. (Symbols) Experimental values of the imaginary part of the third-order susceptibility versus gold layer thickness for (a) 200 fs pulses at a wavelength of 1030 nm and (b) 3 ps pulses at a wavelength of 1064 nm.[26] (Red curves) Thickness dependences obtained using a single fitting parameter D and the nonlinear susceptibility of bulk gold (black lines).

The nonlinear absorption coefficient β is directly connected to the imaginary part of the third-order susceptibility of gold as follows:[27] $\beta \approx \left(3\omega\theta_{\mathrm{Au}}\,\mathrm{Im}[\chi^{(3)}_{\mathrm{Au}}]\right)\Big/\left(2\varepsilon_0 c^2 n_0^2 A_{\mathrm{eff}}\right)$, where $\omega = 2\pi c/\lambda$ is the light angular frequency, c is the vacuum speed of light, ε_0 is the vacuum permittivity, n_0 is the effective linear refractive index of the LRSPP mode,[27] $\theta_{\mathrm{Au}} = \left(\int_{-t_{\mathrm{Au}}/2}^{t_{\mathrm{Au}}/2} |E_z|^2\, dz\right)\left(\int_{-\infty}^{+\infty} |E_z|^2\, dz\right)^{-1}$ is the field localization parameter of the gold layer,[27] $A_{\mathrm{eff}} = \left(\int_{-\infty}^{+\infty}\int_{-\infty}^{+\infty} |E_z|^2 dydz\right)^2 \left(\int_{-\infty}^{+\infty}\int_{-\infty}^{+\infty} |E_z|^4 dydz\right)^{-1}$ is the effective area of the LRSPP mode,[27] $E_z(y,z)$ is the electric field in the transverse section of the waveguide, y is the in-plane coordinate , and z is the vertical coordinate (Figure 1a). In the formula for the field localization parameter θ_{Au}, the initial two-dimensional integrals over the plasmonic mode area were reduced to one-dimensional integrals over the z-coordinate due to the waveguide symmetry.[27] The only contribution to the effective nonlinear loss parameter β of the LRSPP waveguide mode comes from gold because the photon energy at 1030 nm is less than half the bandgap energies for the adhesion and cladding materials of the waveguide.

Gold layer thickness t_{Au} affects the effective nonlinear absorption coefficient β of the LRSPP mode via the field localization parameter θ_{Au} (which increases with t_{Au}) and mode effective area A_{eff} (which decreases with t_{Au}).[27] However, even when these dependences are taken into account, the observed intrinsic nonlinearity $\chi^{(3)}$ of gold additionally increases with the reduction of the film thickness (Figure 2). Using the experimental values on the imaginary part of the third-order susceptibility of gold, $\mathrm{Im}[\chi^{(3)}_{\mathrm{Au}}]$, for 200 fs pulses, the thickness dependence (Figure 2a, red curve) was obtained as follows:[26,27] $\mathrm{Im}[\chi^{(3)}_{\mathrm{Au}}] = \mathrm{Im}[\chi^{(3)}_{\mathrm{200\ fs,\ bulk}}] + D/t_{\mathrm{Au}}$, where D = (8.3 ± 0.3) × 10^{-27} $\mathrm{m}^3/\mathrm{V}^2$ was the only free parameter in the fit. It represents a confinement factor of the

electrons that effectively enhances the nonlinear response for thinner gold layers. In the fitting equation we fixed $\mathrm{Im}[\chi^{(3)}_{200\ \mathrm{fs,\ bulk}}] = 12 \times 10^{-20}\ \mathrm{m^2/V^2}$ as the asymptotic value, which corresponds to the imaginary part of the third-order susceptibility of bulk gold for 200 fs pulses, obtained from the theory presented below. The obtained values of $\mathrm{Im}[\chi^{(3)}_{\mathrm{Au}}]$ for 200 fs pulses are approximately an order of magnitude smaller than those measured previously for 3 ps pulses (Figure 2b). The same as for femtosecond pulses, the fitting curve for the thickness dependence (Figure 2b, red curve) was obtained using the asymptotic limit value for bulk gold for 3 ps pulses $\mathrm{Im}[\chi^{(3)}_{3\ \mathrm{ps,\ bulk}}] = (297 \times 10^{-20}\ \mathrm{m^2/V^2}$ and $D = (153 \pm 11) \times 10^{-27}\ \mathrm{m^3/V^2}$. The origin of the thickness dependence of the third-order susceptibility of thin gold layers is explained in terms of the free electrons motion in gold taking into account a confinement factor. As the layers thickness t_{Au} approaches nanoscale values, free electrons start to feel the layer boundaries, and the collision frequency of electrons in the metal layer increases comparing to bulk metal. This leads to the dependence of the dielectric permittivity of the metal on the layer thickness.[26,27] In turn, the latter results in effective enhancement of the third-order susceptibility of the gold layer comparing to bulk gold.[26,27]

The third-order susceptibility of bulk gold for different pulse durations was calculated using the two-temperature model (TTM) of the free electron temporal dynamics[18,19] (see Supporting Information for details). Incident light pulses first generate, upon partial absorption, nonthermalized (out of equilibrium) hot electrons, which cannot be described by the electron temperature. These nonthermalized electrons then release their energy to the thermalized hot electrons (described by the elevated electronic temperature). For laser pulses with duration longer than the electron-electron scattering rate (on the order of 10 fs),[36] the third-order susceptibility of gold originates from the interaction of the absorbed light with thermalized gas of

hot electrons. The Gaussian-shape laser pulse $P(\tau)=P_0\exp(-\tau^2/\tau_0^2)$ is absorbed by the metal almost instantaneously so that the mean absorbed power density follows the shape of the incident pulse $P_{\mathrm{A}}(\tau)\propto P(\tau)$ (Figure 3). The absorbed power builds up the energy density stored in the nonthermalized part of the electronic distribution $N(\tau)=[h_{\mathrm{th}}*P_{\mathrm{A}}](\tau)=\int_{-\infty}^{\infty}d\tau' h_{\mathrm{th}}(\tau-\tau')P_{\mathrm{A}}(\tau')$, as shown in the Supporting Information, via the convolution of the mean absorbed power and the electron "thermalization" response function of gold $h_{\mathrm{th}}(\tau)=\Theta(\tau)\tau_{\mathrm{th}}^{-1}e^{-\tau/\tau_{\mathrm{th}}}$, where $\Theta(\tau)$ is the Heaviside step function. The rise of the nonthermalized electron energy density is slightly delayed as the hot electrons release their energy to the lattice and thermalized electrons with a characteristic decay time τ_{th} (approximately 300 fs in gold[18,19]). The electron temperature variation from the ground state is $\Delta T_{\mathrm{e}}(\tau)\propto[h_{\mathrm{T}}*P_{\mathrm{A}}](\tau)$ as derived in the Supporting Information. The electron temperature variation is the convolution of the mean absorbed power and the electron-temperature temporal response function of gold $h_{\mathrm{T}}(\tau)=\Theta(\tau)(\tau_{\mathrm{th}}-\tau_{\mathrm{r}})^{-1}(e^{-\tau/\tau_{\mathrm{th}}}-e^{-\tau/\tau_{\mathrm{r}}})$, where τ_{r} is the relaxation time of the free electrons (approximately 1 ps in gold[18,19]). In the short-pulse limit, $\Delta T_{\mathrm{e}}(\tau)\propto h_{\mathrm{T}}(\tau)$, and the rise of the electron temperature on the leading edge of the pulse is governed by the characteristic decay time of the nonthermalized electrons,[19] while on the trailing edge it is governed by the characteristic decay time τ_{r} of the thermalized electrons. Then increased electron temperature $\Delta T_{\mathrm{e}}(\tau)$ dissipates on a multiple-picosecond scale until the ground state thermal equilibrium is reached. Instead, in the long-pulse limit $\Delta T_{\mathrm{e}}(\tau)\propto P_{\mathrm{A}}(\tau)\propto P(\tau)$, and the characteristic time scales of the electron dynamics become too fast for a long pulse to experience any effects of the delayed responses, therefore, it experiences a quasi-instantaneous nonlinear response from the hot thermalized electrons.[18]

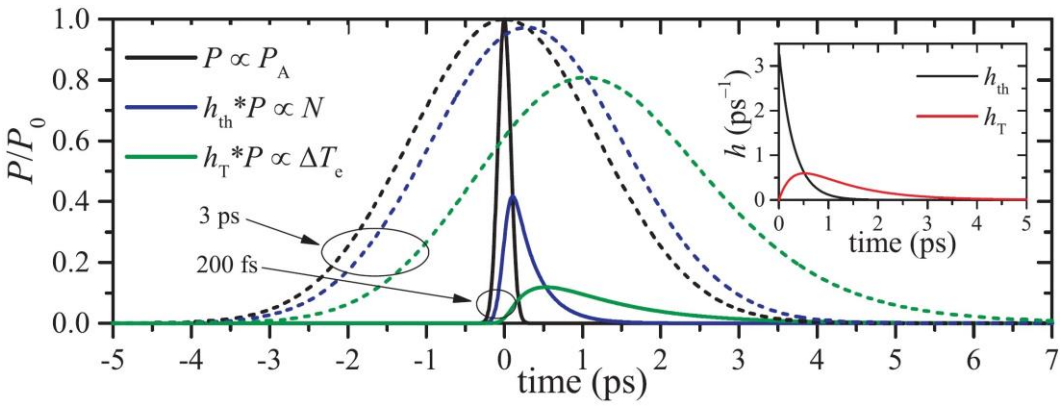

Figure 3. Electron temporal dynamics in bulk gold for 200 fs (solid lines) and 3 ps Gaussian pulses (dashed lines). When pump power P is absorbed in gold, giving the absorbed power density P_A, the latter then creates the nonthermalized electron density N by the electron "thermalization" response function h_{th} (inset). The nonthermalized electrons then convert to the thermalized hot electrons represented by the electron temperature deviation ΔT_e from the lattice temperature. P and ΔT_e are ultimately directly connected by the electron-temperature temporal response function h_T (inset).

Taking into account that the IR wavelengths used in the experiments, namely 1030 and 1064 nm, are far from the strongly dispersive interband transitions,[19] the nonlinear dynamics of the LRSPP mode in the strip plasmonic waveguides can be described with the following nonlinear Schrödinger equation (NLSE) as shown in the Supporting Information:

$$(i\partial_\zeta + D_\tau + i\frac{\alpha}{2})A + (\gamma_{cw} + i\beta_{cw})A[h_T * |A|^2] = 0, \quad \textbf{(1)}$$

where $A(\zeta,\tau)$ is the pulse complex amplitude, ζ and τ are the propagation and time coordinates in the moving frame of the input pulse, $\gamma_{cw} \propto \mathrm{Re}(\chi^{(3)}_{cw})/A_{eff}$ and $\beta_{cw} \propto \mathrm{Im}(\chi^{(3)}_{cw})/A_{eff}$ are the effective nonlinear parameters of the LRSPP mode related to self-phase modulation and two-photon absorption, respectively, in the long-pulse (cw) limit, and D_τ accounts for chromatic dispersion. We see that the electron temperature response function h_T is acting like a

noninstantaneous "delayed" nonlinear response. Using the standard expression $A(\zeta,\tau)=P^{1/2}(\zeta,\tau)\exp[\mathrm{i}\phi(\zeta,\tau)]$, where $P(\zeta,\tau)$ is the pulse power amplitude, and $\phi(\zeta,\tau)$ is the pulse nonlinear phase, the imaginary part of Eq. (1) becomes: $(\partial_\zeta + D_\tau + \alpha)P + \beta_{\mathrm{cw}}P[h_T * P] = 0$. In the cw limit, power P factors out of the convolution, and the equation reduces to the standard nonlinear power equation: $\partial_\zeta P = -\alpha P - \beta_{\mathrm{cw}}P^2$.[27,33]

The situation will be different for ultrashort pulses, for which the continuous wave approximation does not hold. Neglecting the chromatic dispersion for the waveguide lengths and pulse durations considered, we can approximate the convolution as $P[h_{\mathrm{T}} * P](\tau) \approx \rho(\tau_0)P^2(\tau)$. This approximation assumes a temporal overlap between the left side and right side of this expression, which was numerically verified to be satisfied (see Supporting Information). Thus, the nonlinear power equations become:

$$\begin{cases} \partial_\zeta P = -\alpha P - \beta'(\tau_0)P^2, \\ \beta'(\tau_0) = \rho(\tau_0)\beta_{\mathrm{cw}}, \\ \rho(\tau_0) = P_0^{-2}\max_t(P[h_{\mathrm{T}} * P](\tau)), \end{cases} \quad \textbf{(2)}$$

where P_0 is the pulse peak power. This is equivalent to the standard nonlinear power equation[27,33] with an effective nonlinear absorption coefficient $\beta'(\tau_0)$. Correction factor $\rho(\tau_0)$ describes the deviation from the long pulse limit of the nonlinear absorption coefficient due to the noninstantaneous thermal response of free-electrons in metal. It depends on input pulse duration τ_0 and pulse shape, and $\rho(\tau_0)\to 1$ in the cw limit (see Supporting Information). Note that since $P[h_{\mathrm{T}} * P](\tau) \propto P(\tau)\Delta T_{\mathrm{e}}(\tau)$, the correction factor is mainly affected by a temporal overlap between the pulse envelope and the electron temperature variation. The introduction of the correction

factor allows to describe the imaginary part of the third-order susceptibility of gold for arbitrary pulse duration τ_0 as follows:

$$\mathrm{Im}[\chi^{(3)}(\omega_0,\tau_0,t_{\mathrm{Au}})]=\rho(\tau_0)(\mathrm{Im}[\chi^{(3)}_{\mathrm{cw,bulk}}(\omega_0)]+D_{\mathrm{cw}}/t_{\mathrm{Au}}), \quad \textbf{(3)}$$

where t_{Au} is the gold layer thickness and ω_0 is the light angular frequency. $\chi^{(3)}_{\mathrm{cw,bulk}}(\omega_0)$ and D_{cw} are the third-order susceptibility of bulk gold and the correction factor due to the electron confinement, respectively, in the cw limit; these can be calculated[18,19] or determined experimentally. The first term in the brackets is the intrinsic nonlinear susceptibility of bulk gold while the second term is expected to depend on the electron confinement (i.e., whether 1D or 2D nanostructures are considered). In the following, we use the theoretical value $\mathrm{Im}[\chi^{(3)}_{\mathrm{cw,bulk}}(1030\ \mathrm{nm})]=430\times10^{-20}\ \mathrm{m^2/V^2}$.[19]

We can now directly compare the values of the third-order susceptibility of thin gold layers measured in the present work with 200 fs pulses at a wavelength of 1030 nm, and those measured for the same waveguides in Ref. 26 with 3 ps pulses at 1064 nm. This is justified by the fact that both wavelengths, 1030 nm and 1064 nm, are far from the interband transitions in gold[19,20] and close to each other. We calculated the correction factors for Gaussian-shaped input pulses in the range from 10 fs to 10 ps, and as a first verification of eq 3, we show that the relation $D=\rho(\tau_0)D_{\mathrm{cw}}$ indeed holds (see Supporting Information Figure S3). We used the cw fitting coefficient as a free parameter, and the obtained experimental values of D were used to determine $D_{\mathrm{cw}} = 220 \times 10^{-27}\ \mathrm{m^3/V^2}$ (accurate within 10%). Then eq 3 was used to plot the third-order gold susceptibility for different pulse durations for the gold layer thickness t_{Au} = 22, 27, and 35 nm (Figure 4a). We see that in all three cases, eq 3 represents quantitatively the measured

data, thus justifying the introduction of the correction factor, and also validating the theoretical value of the third-order susceptibility of bulk gold in the cw limit. Note that the correction factor $\rho(\tau_0)$ is only needed to connect experimentally measured values of the nonlinearity with the nonlinear refraction and nonlinear absorption coefficients in the cw limit. Once these values are determined, they are used in the NLSE in eq 1 and the need for the correction factor vanishes. A similar relation as eq 3 can be derived in the model for the real part of the third-order susceptibility of gold (Figure 4b), which governs self-phase modulation effects. The plot in Figure 4b uses the theoretical value of Re[$\chi^{(3)}_{\mathrm{cw,bulk}}(\omega_0)$] for bulk gold as the saturation value in the long-pulse limit and the thickness dependence in the cw limit is calculated using the experimental data for 3 ps pulses. This approach is, therefore, based on the behavior observed for the imaginary part of the third-order susceptibility (Figure 4a) for which these parameter choices and the use of the correction factor were experimentally confirmed. The theoretical curves for the real part of the third-order susceptibility indeed match the experimental data for 3 ps pulses, but further experiments are needed to exactly verify the predicted behavior. Nevertheless, a general trend of the decreased nonlinearity for shorter pulses is in line with the literature data.[20]

The predicted variation of the third-order susceptibility of gold monotonically spans over about 4 orders of magnitude as the pulse duration changes from 10 fs to 10 ps (Figure 4). The obtained pulse duration dependences are in good agreement with previous studies,[20] where the experimental values of the third-order nonlinear susceptibility for bulk gold were summarized from different experiments. Such a variation of the third-order nonlinearity of gold with respect to the signal pulse duration can be one of the principal advantages of free electron nonlinearities in plasmonic waveguides compared to conventional dielectric nonlinearities for the realization of ultrafast nanophotonic components.[2,3]

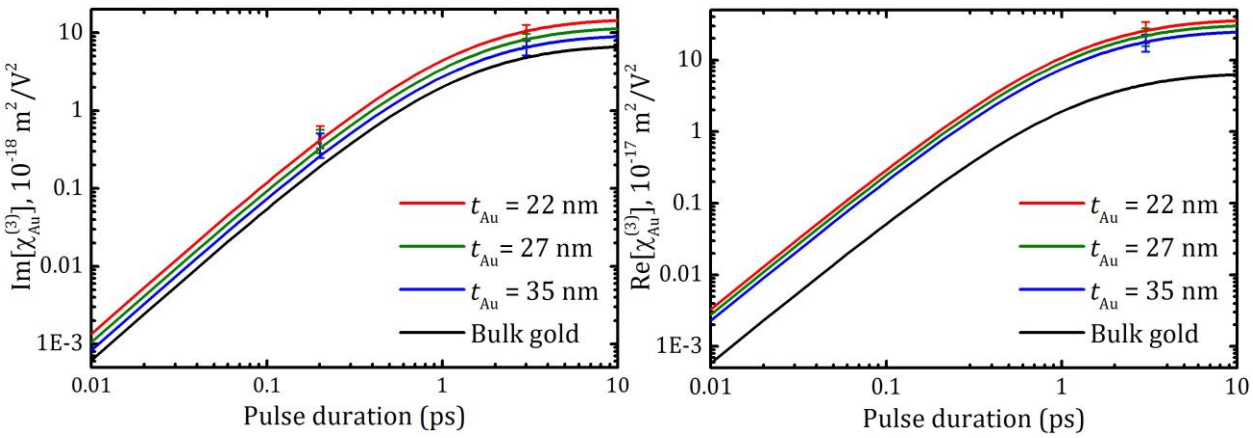

Figure 4. Theoretical pulse duration dependences of (a) imaginary part and (b) real part of the third-order susceptibility of gold layers with t_{Au} = 22, 27, and 35 nm and bulk gold. (Symbols) The experimental data measured with 200 fs pulses at a wavelength of 1030 nm (present work) and 3 ps pulses at 1064 nm.[26] It should be noted that the theoretical curves in (b) use the cw limit value of the third-order susceptibility taken from the theory, and, therefore, the shown pulse-duration trend is only indicative; further experiments are needed to exactly verify the predicted behavior.

In summary, we have shown that nonlinear dynamics of the long-range surface plasmon polariton mode in the gold strip waveguides significantly depends on both the gold layer thickness and the laser pulse duration. In particular, the origin of the pulse duration dependence has been explained in detail by studying the electron temporal dynamics using the two-temperature model, which infers that a picosecond pulse interacts with metal stronger than a femtosecond pulse because of greater temporal overlaps of the laser pulse with the excited electron gas. Consequently, this leads to higher values of the third-order nonlinearity for longer pulses, as expressed by the correction factor in Eq. 2. Importantly, the experimental data on nonlinear absorption validate the connection between the characteristic response function of gold derived in the TTM and its role as a "delayed" nonlinearity for an ultrafast LRSPP mode in the

framework of a nonlinear Schrödinger equation. The response function of gold is purely based on characteristic time scales of the electron-gas relaxation, and a correction factor, Eq. 2, is introduced to gauge the magnitude of the delayed temperature nonlinear response for pulse durations shorter than or comparable to the electron relaxation times and, thus, connect the experimental measurements with theoretical results. The thickness dependence is explained in terms of the free electrons motion in gold taking into account confinement factor of the electrons, which we determine experimentally. The collision frequency of electrons in thin gold layers increases comparing to bulk gold, and it leads to enhancement of the effective third-order nonlinear susceptibility.[26,27] The developed theoretical approach can be used to determine the third-order nonlinear susceptibility of free-electron gas in metals for any wavelength, pulse duration and metal layer thickness, once the nonlinear susceptibility of bulk metal for cw excitation are known and the electron-confinement enhancement factor is determined experimentally for a particular type of nanostructure.

In future it will be important to investigate the linear and nonlinear optical properties of the waveguides with even thinner gold layers (up to ~10 nm). The standard Drude model breaks down at the metal layer thicknesses below 10 nm due to possible nonlocal[37,38] and quantum effects.[39,40] Also there is a clustering process for thin metal layers,[41] and their fabrication especially with thicknesses below 10 nm is challenging.[42] Thus, a complete hydrodynamic description, including nonlocal effects is required, which is especially important in the nonlinear regime.[43,44]

The presented results on nonlinear optical properties of long-range surface plasmon polaritons in the gold strip waveguides can be exploited for the development and applications of active

plasmonic and nanophotonic components, and for accurate *a priori* modeling of ultrafast nanoplasmonic devices.

Supporting Information.

The details of the experimental setup, the two-temperature model of electron temporal dynamics in gold, and the obtained experimental and theoretical values of the third-order susceptibility of gold are presented. This material is available free of charge via the Internet at http://pubs.acs.org.

Corresponding Author

*E-mail: ollyse@fotonik.dtu.dk.

Present Address

|| The University of Sheffield, Sheffield S10 2TN, UK.

Author Contributions

§ O. Lysenko and M. Bache contributed equally.

Funding Sources

EPSRC (UK) grants EP/H000917/2, EP/J018457/1 and EP/M013812/1.

ACKNOWLEDGMENT

This work was supported, in part, by EPSRC (UK). A.V.Z. acknowledges support from the Royal Society and the Wolfson Foundation. The data access statement: all data supporting this research are provided in full in the results section and supporting information.

REFERENCES

(1) Brongersma, M. L.; Shalaev, V. M. The Case for Plasmonics. *Science* **2010**, *328*, 440-441.

(2) Bozhevolnyi, S. I. *Plasmonic Nanoguides and Circuits*; Pan Stanford: 2009.

(3) Krasavin, A. V.; Zayats, A. V. Active Nanophotonic Circuitry Based on Dielectric-Loaded Plasmonic Waveguides. *Adv. Opt. Mater.* **2015**, *3*, 1662-1690.

(4) Gramotnev, D. K.; Bozhevolnyi, S. I. Plasmonics Beyond the Diffraction Limit. *Nat. Photonics* **2010**, *4*, 83-91.

(5) Zenin, V. A.; Andryieuski, A.; Malureanu, R.; Radko, I. P.; Volkov, V. S.; Gramotnev, D. K.; Lavrinenko, A. V.; Bozhevolnyi, S. I. Boosting Local Field Enhancement by on-Chip Nanofocusing and Impedance-Matched Plasmonic Antennas. *Nano Lett.* **2015**, *15*, 8148-8154.

(6) Krupin, O.; Asiri, H.; Wang, C.; Tait, R. N.; Berini, P. Biosensing Using Straight Long-Range Surface Plasmon Waveguides. *Opt. Express* **2013**, *21*, 698-709.

(7) Berini, P. Bulk and Surface Sensitivities of Surface Plasmon Waveguides. *New J. Phys.* **2008**, *10*, 105010.

(8) De Leon, I.; Berini, P. Amplification of Long-Range Surface Plasmons by a Dipolar Gain Medium. *Nat. Photonics* **2010**, *4*, 382-387.

(9) Berini, P.; De Leon, I. Surface Plasmon-Polariton Amplifiers and Lasers. *Nat. Photonics* **2012**, *6*, 16-24.

(10) Diaz, F. J.; Li, G.; Martijn de Sterke, C.; Kuhlmey, B. T.; Palomba, S. Kerr Effect in Hybrid Plasmonic Waveguides. *J. Opt. Soc. Am. B* **2016**, *33*, 957-962.

(11) Diaz, F. J.; Hatakeyama, T.; Rho, J.; Wang, Y.; O'Brien, K.; Zhang, X.; Martijn de Sterke, C.; Kuhlmey, B. T.; Palomba, S. Sensitive Method for Measuring Third Order Nonlinearities in Compact Dielectric and Hybrid Plasmonic Waveguides. *Opt. Express* **2016**, *24*, 545-554.

(12) Kauranen M.; Zayats, A. V. Nonlinear Plasmonics. *Nat. Photonics* **2012**, *6*, 737-748.

(13) Neira, A. D.; Olivier, N.; Nasir, M. E.; Dickson, W.; Wurtz, G. A.; Zayats, A. V. Eliminating Material Constraints for Nonlinearity with Plasmonic Metamaterials. *Nat. Commun.* **2015**, *6*, 7757.

(14) Lassiter, J. B.; Chen, X.; Liu, X.; Ciracì, C.; Hoang, T. B.; Larouche, S.; Oh, S.-H.; Mikkelsen, M. H.; Smith, D. R. Third-Harmonic Generation Enhancement by Film-Coupled Plasmonic Stripe Resonators. *ACS Photonics* **2014**, *1*, 1212-1217.

(15) Butet, J.; Brevet, P.-F.; Martin, O. J. F. Optical Second Harmonic Generation in Plasmonic Nanostructures: From Fundamental Principles to Advanced Applications. *ACS Nano* **2015**, *9*, 10545-10562.

(16) Ginzburg, P.; Krasavin, A. V.; Zayats, A. V. Cascaded Second-Order Surface Plasmon Solitons Due to Intrinsic Metal Nonlinearity. *New J. Phys.* **2013**, *15*, 013031.

(17) O'Donnell, K. A.; Torre, R. Characterization of the Second-Harmonic Response of a Silver-Air Interface. *New J. Phys.* **2005**, *7*, 154.

(18) Conforti M.; Della Valle, G. Derivation of Third-Order Nonlinear Susceptibility of Thin Metal Films as a Delayed Optical Response. *Phys. Rev. B* **2012**, *85*, 245423.

(19) Marini, A.; Conforti, M.; Della Valle, G.; Lee, H. W.; Tran, Tr. X.; Chang, W.; Schmidt, M. A.; Longhi, S.; Russell, P. St. J.; Biancalana, F. Ultrafast Nonlinear Dynamics of Surface Plasmon Polaritons in Gold Nanowires Due to the Intrinsic Nonlinearity of Metals. *New J. Phys.* **2013**, *15*, 013033.

(20) Boyd, R. W.; Shi, Z.; De Leon, I. The Third-Order Nonlinear Optical Susceptibility of Gold. *Opt. Commun.* **2014**, *326*, 74-79.

(21) Rotenberg, N.; Bristow, A. D.; Pfeiffer, M.; Betz, M.; van Driel, H. M. Nonlinear Absorption in Au Films: Role of Thermal Effects. *Phys. Rev. B* **2007**, *75*, 155426.

(22) Smith, D. D.; Yoon, Y.; Boyd, R. W.; Campbell, J. K.; Baker, L. A.; Crooks, R. M.; George, M. Z-Scan Measurement of the Nonlinear Absorption of a Thin Gold Film. *J. Appl. Phys.* **1999**, *86*, 6200-6205.

(23) Lee, T. K.; Bristow, A. D.; Hübner, J.; van Driel, H. M. Linear and Nonlinear Optical Properties of Au-Polymer Metallodielectric Bragg Stacks. *J. Opt. Soc. Am. B* **2006**, *23*, 2142-2147.

(24) Xenogiannopoulou, E.; Aloukos, P.; Couris, S.; Kaminska, E.; Piotrowska, A.; Dynowska, E. Third-Order Nonlinear Optical Properties of Thin Sputtered Gold Films. *Opt. Commun.* **2007**, *275*, 217-222.

(25) Meier, S. A. *Plasmonics: Fundamentals and Applications*; Springer: 2007.

(26) Lysenko, O.; Bache, M.; Lavrinenko, A. Third-Order Susceptibility of Gold for Ultrathin Layers. *Opt. Lett.* **2016**, *41*, 317-320.

(27) Lysenko, O.; Bache, M.; Lavrinenko, A. Nonlinear Optical Model for Strip Plasmonic Waveguides. *J. Opt. Soc. Am. B* **2016**, *33*, 1341-1348.

(28) Agrawal, G. P. *Nonlinear Fiber Optics*; Elsevier: 2013.

(29) Bright, T. J.; Watjen, J. I.; Zhang, Z. M.; Muratore, C.; Voevodin, A. A.; Koukis, D. I.; Tanner, D. B.; Arenas, D. J. Infrared Optical Properties of Amorphous and Nanocrystalline Ta_2O_5 Thin Films. *J. Appl. Phys.* **2013**, *114*, 083515.

(30) Tai, C. Y.; Wilkinson, J. S.; Perney, N. M. B.; Netti, M. C.; Cattaneo, F.; Finlayson, C. E.; Baumberg, J. J. Determination of Nonlinear Refractive Index in a Ta_2O_5 Rib Waveguide Using Self-Phase Modulation. *Opt. Express* **2004**, *12*, 5110-5116.

(31) Habteyes, T. G.; Dhuey, S.; Wood, E.; Gargas, D.; Cabrini, S.; Schuck, P. J.; Alivisatos P. A.; Leone, S. R. Metallic Adhesion Layer Induced Plasmon Damping and Molecular Linker as a Nondamping Alternative. *ACS Nano* **2012**, *6*, 5702-5709.

(32) Klimov, V. *Nanoplasmonics*; Pan Stanford: 2014.

(33) Boyd, R. W. *Nonlinear Optics*; Elsevier: 2008.

(34) Dryzek, J.; Czapla, A. Quantum Size Effect in Optical Spectra of Thin Metallic Films. *Phys. Rev. Lett.* **1987**, *58*, 721-724.

(35) Zayats, A. V.; Keller, O; Pedersen, K.; Liu, A.; Pudonin F. A. Linear Optical Properties and Second-Harmonic Generation from Ultrathin Niobium Films: A Search for Quantization Effects, *IEEE J. Quantum Electron*. **1995**, *31*, 2044-2051.

(36) Kittel, C. *Introduction to Solid State Physics*; Wiley: 2005.

(37) Raza, S.; Bozhevolnyi, S. I.; Wubs, M.; Mortensen, N. A. Nonlocal Optical Response in Metallic Nanostructures. *J. Phys. Condens. Matter* **2015**, *27*, 183204.

(38) Ginzburg, P.; Zayats, A. V. Localized Surface Plasmon Resonances in Spatially Dispersive Nano-Objects: Phenomenological Treatise. *ACS Nano* **2013**, *7*, 4334-4342.

(39) Qian, H.; Xiao, Y.; Lepage, D.; Chen, L.; Liu, Z. Quantum Electrostatic Model for Optical Properties of Nanoscale Gold Films. *Nanophotonics* **2015**, *4*, 413-418.

(40) Su, W. B.; Chang, C. S.; Tsong, T. T. Quantum Size Effect on Ultra-Thin Metallic Films. *J. Phys. D: Appl. Phys.* **2010**, *43*, 013001.

(41) Kreibig U.; Vollmer, M. *Optical Properties of Metal Clusters*; Springer: 1995.

(42) Malureanu, R.; Lavrinenko, A. Ultra-Thin Films for Plasmonics: a Technology Overview. *Nanotechnol. Rev.* **2015**, *4*, 1-17.

(43) Ginzburg, P.; Krasavin, A. V.; Wurtz, G. A.; Zayats, A. V. Nonperturbative Hydrodynamic Model for Multiple Harmonics Generation in Metallic Nanostructures. *ACS Photonics* **2015**, *2*, 8-13.

(44) Krasavin, A. V.; Ginzburg, P.; Wurtz, G. A.; Zayats, A. V. Nonlocality-Driven Supercontinuum White Light Generation in Plasmonic Nanostructures. *Nat. Comm.* **2016**, *7*, 11497.

For Table of Contents Only.

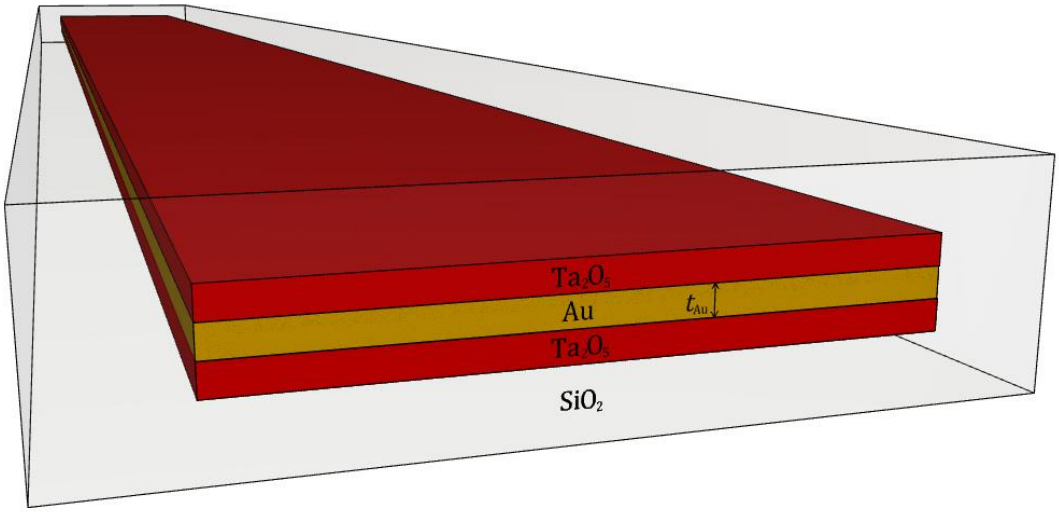

Supporting Information: Nonlinear Dynamics of Ultrashort Long-Range Surface Plasmon Polariton Pulses in Gold Strip Waveguides

Oleg Lysenko,[*,†,§] *Morten Bache,*[†,§] *Nicolas Olivier,*[‡,∥] *Anatoly V. Zayats,*[‡] *and Andrei Lavrinenko*[†]

[†]Department of Photonics Engineering, Technical University of Denmark, Oersteds Plads, Building 345 V, Kongens Lyngby 2800, Denmark

[‡]Department of Physics, King's College London, Strand, London WC2R 2LS, UK

S1. Experimental Setup

The experimental setup is shown in Figure S1. The laser source was the femtosecond laser amplifier PHAROS (Light Conversion), providing ~200 fs FWHM pulses with a tunable repetition rate here set at 200 kHz at a center wavelength of 1030 nm. The average power of the free-space laser beam was tuned by several neutral density (ND) filters, and the linear polarization of the beam was aligned by a half-wave plate and linear polarizer to match the transverse magnetic polarization of the long-range surface plasmon polariton (LRSPP) mode in the plasmonic waveguides. The end-fire coupling method was used to excite the plasmonic modes.[1] An iris diaphragm was placed to eliminate the scattered light and to transmit the plasmonic mode optical flux to the power meter S132C (Thorlabs). The alignment of the samples

and the end-fire coupling were controlled by using the digital color camera WAT-221S (Watec). Before the transmission measurements were taken, the LRSPP mode in each waveguide was imaged by the digital camera DCC1240M (Thorlabs) and the transverse magnetic polarization of the plasmonic mode was verified using the half-wave plate and linear polarizer.[2] This polarization check verified coupling to the LRSPP mode in each plasmonic waveguide.

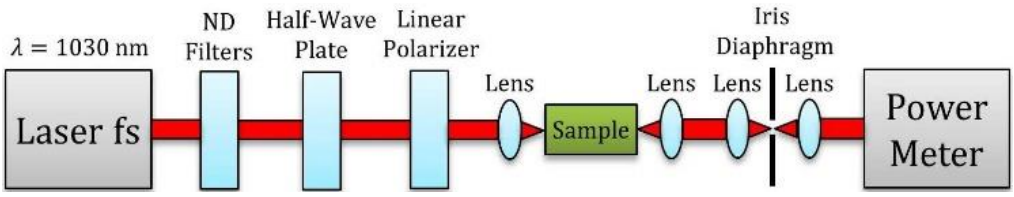

Figure S1. Experimental setup for nonlinear optical measurements.

The nonlinear propagation of the LRSPP mode in the plasmonic waveguides was characterized by tuning the input average power of the free-space laser beam right before the waveguides from 1 mW (5 nJ) to about 55 mW (275 nJ). By using the measured values of the coupling loss *C* (approximately 3.5 dB per facet), the corresponding values of the pulse energy and peak power inside the waveguides were therefore in the range 2-120 nJ and 10-600 kW, respectively. Any further increase of the average power of the free-space laser beam caused significant heating and melting of the waveguide structures.

S2. Electron Temporal Dynamics in Gold

The experimental values of the imaginary part of the third-order nonlinear susceptibility $\chi_{\mathrm{Au}}^{(3)}$ of the gold layers in the strip plasmonic waveguides for 200 fs pulses are significantly smaller than

the values of the imaginary part of $\chi^{(3)}_{\mathrm{Au}}$ obtained previously with 3 ps pulses.[3] We applied the two-temperature model (TTM) of free electron temporal dynamics in gold[4,5] to explain the obtained experimental results on the imaginary part of $\chi^{(3)}_{\mathrm{Au}}$ and also to estimate the values of the real part of $\chi^{(3)}_{\mathrm{Au}}$ for 200 fs pulses. The theoretical dependences of the third-order nonlinear susceptibility of gold were expanded for the wide range of the pulse duration from 10 fs to 10 ps.

To introduce the TTM of free electron temporal dynamics in gold, let us consider an ultrashort optical pulse with the Gaussian electric field profile $E(\tau)=E_0 e^{-\tau^2/(2\tau_0^2)}e^{-i\omega\tau}$, where E_0 is the electric field amplitude, ω is the light angular frequency, t is the time coordinate, $\tau_0=\Delta\tau/(2\sqrt{\ln(2)})$ is the 1/e intensity half-width, and $\Delta\tau$ is the pulse full-width at half maximum (FWHM). The mean absorbed power per unit volume of gold $P_{\mathrm{A}}(\tau)$ is given by:[4]

$$P_{\mathrm{A}}=\frac{\varepsilon_0\omega|E_0|^2}{2}\mathrm{Im}[\varepsilon_{\mathrm{Au}}]e^{-\tau^2/\tau_0^2}-\frac{\tau\varepsilon_0|E_0|^2}{2\tau_0^2}e^{-\tau^2/\tau_0^2}\left(1+\frac{\omega_{\mathrm{p}}^2(\omega^2-\gamma^2)}{(\omega^2+\gamma^2)^2}\right), \qquad \textbf{(S1)}$$

where $\omega_{\mathrm{p}}=\sqrt{ne^2/\varepsilon_0 m_{\mathrm{e}}}$ is the plasma frequency for gold, e is the electron charge, ε_0 is the vacuum permittivity, n is the electron density, m_{e} is the electron mass, γ is the collision frequency of electrons for bulk gold, and $\varepsilon_{\mathrm{Au}}$ is the dielectric permittivity for bulk gold. Since the pulse carrier frequency is far from the interband transitions in gold, it is straightforward to show that Eq. S1 can be simplified as follows $P_{\mathrm{A}}\approx(1/2)\varepsilon_0\omega|E_0|^2\,\mathrm{Im}[\varepsilon_{\mathrm{Au}}]\exp(-\tau^2/\tau_0^2)$. Then this expression is used to solve the equations of the free electron temporal dynamics:[4,5]

$$\begin{cases} \dfrac{\partial N}{\partial \tau} = -(\gamma_{\mathrm{e}} + \gamma_{\mathrm{lat}})N + P_{\mathrm{A}}, \\ C_{\mathrm{e}} \dfrac{\partial T_{\mathrm{e}}}{\partial \tau} = C(T_{\mathrm{lat}} - T_{\mathrm{e}}) + \gamma_{\mathrm{e}} N, \\ C_{\mathrm{lat}} \dfrac{\partial T_{\mathrm{lat}}}{\partial \tau} = C(T_{\mathrm{e}} - T_{\mathrm{lat}}) + \gamma_{\mathrm{lat}} N, \end{cases} \quad \textbf{(S2)}$$

where $T_{\mathrm{e}}(\tau)$ is the electronic temperature, $T_{\mathrm{lat}}(\tau)$ is the lattice temperature, C_{e} = 2.1 × 10^4 J m^{-3} K^{-1} is the electronic heat capacity per unit volume of gold,[6] C_{lat} = 2.5 × 10^6 J m^{-3} K^{-1} is the lattice heat capacity per unit volume of gold,[6] γ_{e} = 2 × 10^{12} s^{-1} is the electron thermalization rate,[7] γ_{lat} = 1 × 10^{12} s^{-1} is the lattice thermalization rate,[7] C = 2 × 10^{16} s^{-1} is the electron-photon coupling coefficient,[6] and $N(\tau)$ is the energy density stored in the nonthermalized part of the electronic distribution.[4]

This system of differential equations can be solved directly in the frequency domain[4,5]. After the Fourier transform of Eq. S2, the following equations are obtained:

$$\begin{cases} -i\omega\tau_{\mathrm{th}}\tilde{N} = -(\gamma_{\mathrm{e}} + \gamma_{\mathrm{lat}})\tilde{N} + \tilde{P}_{\mathrm{A}}, \\ -i\omega C_{\mathrm{e}}\tilde{T}_{\mathrm{e}} = C(\tilde{T}_{\mathrm{lat}} - \tilde{T}_{\mathrm{e}}) + \gamma_{\mathrm{e}}\tilde{N}, \\ -i\omega C_{\mathrm{lat}}\tilde{T}_{\mathrm{lat}} = C(\tilde{T}_{\mathrm{e}} - \tilde{T}_{\mathrm{lat}}) + \gamma_{\mathrm{lat}}\tilde{N}, \end{cases} \quad \textbf{(S3)}$$

where the tilde character ("~") denotes the Fourier transform of a function. The solution to the first equation of the system (Eq. S3) in the frequency and time domains is as follows:

$$\begin{aligned} \tilde{N}(\omega) &= \tilde{h}_{\mathrm{th}}(\omega)\tilde{P}_{\mathrm{A}}(\omega), \\ N(\tau) &= [h_{\mathrm{th}} * P_{\mathrm{A}}](\tau), \end{aligned} \quad \textbf{(S4)}$$

where $[f*g](\tau)=\int_{-\infty}^{\infty}d\tau' f(\tau')g(\tau-\tau')$ denotes the convolution of two functions (*f* and *g*). We applied the following convolution theorem:

$$[f*g](\tau)=(2\pi)^{-1}\int_{-\infty}^{\infty}d\omega e^{i\omega\tau}\tilde{f}(\omega)\tilde{g}(\omega). \quad \textbf{(S5)}$$

In Eq. S4 the thermalization response function of gold[5] in the frequency and time domains is as follows:

$$\begin{aligned}\tilde{h}_{\mathrm{th}}(\omega)&=(1-i\omega\tau_{\mathrm{th}})^{-1},\\ h_{\mathrm{th}}(\tau)&=\Theta(\tau)\tau_{\mathrm{th}}{}^{-1}e^{-\tau/\tau_{\mathrm{th}}},\end{aligned} \quad \textbf{(S6)}$$

where $\Theta(\tau)$ is the Heaviside step function and $\tau_{\mathrm{th}}=1/(\gamma_{\mathrm{e}}+\gamma_{\mathrm{lat}})$ is the characteristic decay time of the energy density of the nonthermalized part of the electronic distribution[4] (approximately 300 fs in gold). From the second and third equations of the system (Eq. S3) the electron temperature variation $\Delta T_{\mathrm{e}}(\tau)=T_{\mathrm{e}}(\tau)-T_{\mathrm{lat}}(\tau)$ in the frequency domain is given by:

$$\Delta\tilde{T}_{\mathrm{e}}(\omega)=\tau_{\mathrm{r}}(\gamma_{\mathrm{e}}/C_{\mathrm{e}}-\gamma_{\mathrm{lat}}/C_{\mathrm{lat}})\tilde{N}(\omega)(1-i\omega\tau_{\mathrm{r}})^{-1}, \quad \textbf{(S7)}$$

where $\tau_{\mathrm{r}}=C_{\mathrm{e}}C_{\mathrm{lat}}/[C(C_{\mathrm{e}}+C_{\mathrm{lat}})]$ is the characteristic decay time of the thermalized electrons[4,5] (approximately 1 ps in gold). The expression for the electron temperature variation in the frequency and time domains is as follows:

$$\begin{aligned}\Delta\tilde{T}_{\mathrm{e}}(\omega)&=\tau_{\mathrm{r}}\tau_{\mathrm{th}}(\gamma_{\mathrm{e}}/C_{\mathrm{e}}-\gamma_{\mathrm{lat}}/C_{\mathrm{lat}})\tilde{h}_{\mathrm{T}}(\omega)\tilde{P}_{\mathrm{A}}(\omega),\\ \Delta T_{\mathrm{e}}(\tau)&=\tau_{\mathrm{r}}\tau_{\mathrm{th}}(\gamma_{\mathrm{e}}/C_{\mathrm{e}}-\gamma_{\mathrm{lat}}/C_{\mathrm{lat}})[h_{\mathrm{T}}*P_{\mathrm{A}}](\tau),\end{aligned} \quad \textbf{(S8)}$$

where h_{T} is the temperature response function of gold:[4,5]

$$\tilde{h}_{\mathrm{T}}(\omega)=(1-i\omega\tau_{\mathrm{r}})^{-1}(1-i\omega\tau_{\mathrm{th}})^{-1},$$
$$h_{\mathrm{T}}(\tau)=\Theta(\tau)(\tau_{\mathrm{th}}-\tau_{\mathrm{r}})^{-1}(e^{-\tau/\tau_{\mathrm{th}}}-e^{-\tau/\tau_{\mathrm{r}}}). \quad \textbf{(S9)}$$

It is important to note that $\tilde{h}_{\mathrm{T}}(\omega)=\tilde{h}_{\mathrm{th}}(\omega)(1-i\omega\tau_{\mathrm{r}})^{-1}$, therefore, the temporal response function of gold also contains the thermalization response function h_{th}. This is because the energy density of the nonthermalized electrons *N* acts as an intermediate stage between the absorbed power and the hot thermalized electron dynamics, and it only indirectly enters into the final equation for the electron temperature variation (Eq. S8). The thermalization response function h_{th} and the temporal response function h_{T} in the time and frequency domains are shown in Figure S2. Functions h_{th} and h_{T} were calculated using the characteristic decay times $\tau_{\mathrm{th}}=0.3\,\mathrm{ps}$, and $\tau_{\mathrm{r}}=1\,\mathrm{ps}$.

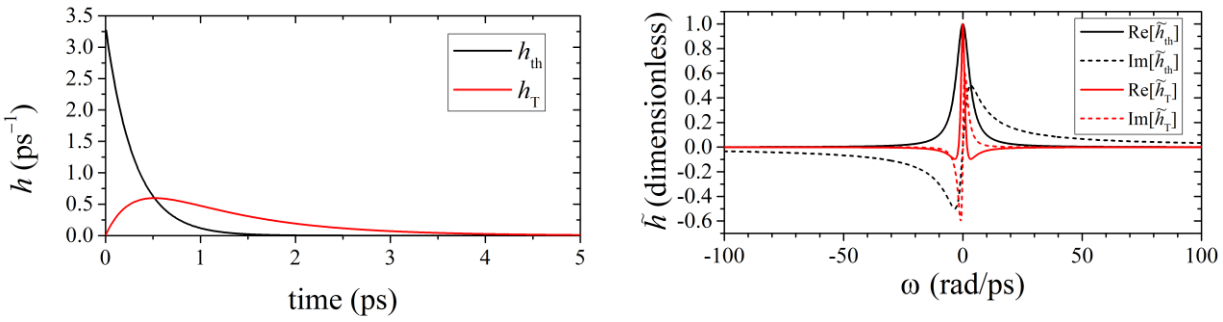

Figure S2. Thermalization and temporal response functions of gold in the time and frequency domains.

S3. Nonlinear Schrödinger Equation

The propagation dynamics of the LRSPP mode in the strip plasmonic waveguides is well described by the nonlinear Schrödinger equation (NLSE),[8] following the classical nonlinear fiber optics formalism.[9] A general form of the NLSE is

$$(i\partial_\zeta + D_\tau + i\frac{\alpha}{2})A(\zeta,\tau) + \gamma_{\mathrm{cw}}A(\zeta,\tau)[R_\gamma * |A|^2](\zeta,\tau) + i\beta_{\mathrm{cw}}A(\zeta,\tau)[R_\beta * |A|^2](\zeta,\tau) = 0, \quad \textbf{(S10)}$$

where $R_\gamma(\tau) = (1-f_\gamma)\delta(\tau) + f_\gamma h_\gamma(\tau)$ and $R_\beta(\tau) = (1-f_\beta)\delta(\tau) + f_\beta h_\beta(\tau)$ are the generalized temporal response functions of the real and imaginary parts of the third-order nonlinear susceptibility of gold,[8,10] respectively, ζ and τ are the propagation and time coordinates in the moving frame of the pump pulse,[8] the chromatic dispersion term is[8] $D_\tau = \sum_{m=2}^{\infty} m!^{-1} i^m \beta_m(\omega_0)\frac{\partial^m}{\partial\tau^m}$, where $\beta_m(\omega_0) = \frac{\partial^m \beta(\omega_0)}{\partial\omega^m}$, and the field is normalized so that $|A|^2$ is related to the power in watts.

The gold layer has the dominant contribution to both the real and imaginary parts of the effective third-order susceptibility of the LRSPP mode.[3,9] The non-instantaneous contribution terms to the nonlinear gamma-parameter and nonlinear absorption coefficient in Eq. S10 can be described by using the electron temperature variation $\Delta T_e(\tau) \propto [h_\Gamma * P](\tau)$ and $R_\gamma(\tau) = R_\beta(\tau) = h_\Gamma(\tau)$. Thus, the NLSE has the following form:[4]

$$(i\partial_\zeta + D_\tau + i\frac{\alpha}{2})A(\zeta,\tau) + (\gamma_{\mathrm{cw}} + i\beta_{\mathrm{cw}})A(\zeta,\tau)[h_\Gamma * |A|^2](\zeta,\tau) = 0 \qquad \textbf{(S11)}$$

The nonlinear terms here are separated into the real and imaginary parts, describing self-phase modulation and nonlinear (two-photon) absorption, respectively. The subscript "cw" denotes the nonlinear coefficients in the long-pulse (continuous wave) limit, because in this regime

$[h_T * |A|^2](\tau) \approx |A(\tau)|^2 \int_{-\infty}^{\infty} d\tau' h_T(\tau') = |A(\tau)|^2$, and the contributions from the non-instantaneous nonlinear response vanish. The temporal response function of gold is normalized so that its integral over time is unity.

S4. Correction Factor

The introduction of the correction factor is justified below. Let us focus on the nonlinear absorption term in Eq. S11. After the standard substitution $A(\zeta,\tau) = \sqrt{P(\zeta,\tau)}\exp[i\phi(\zeta,\tau)]$, the imaginary part of the NLSE becomes

$$(\partial_\zeta + D_\tau + \alpha)P(\zeta,\tau) + \beta_{cw}P(\zeta,\tau)[h_T * P](\zeta,\tau) = 0. \quad \textbf{(S12)}$$

In the cw limit, the imaginary part of the NLSE reduces to the standard nonlinear equation[9,10] $\partial_\zeta P = -\alpha P - \beta_{cw}P^2$, which has the following solution[9]:

$$P(L,\tau) = P_0(\tau)e^{-\alpha L}/[1 + \beta_{cw}L_{eff}P_0(\tau)]. \quad \textbf{(S13)}$$

where $P_0(\tau)$ is the power at ζ = 0 and $L_{eff} = (1 - e^{-L\alpha})/\alpha$ is the effective length with L being the physical propagation length.

The next step is to obtain a similar expression for ultrashort pulses. The chromatic dispersion can be neglected for the waveguide lengths and pulse durations considered here, therefore, if we approximate:

$$P(\zeta,\tau)[h_T * P](\zeta,\tau) \approx \rho(\tau_0)P^2(\zeta,\tau), \quad \textbf{(S14)}$$

equation S12 becomes:

$$\partial_\zeta P = -\alpha P - \beta'(\tau_0) P^2, \tag{S15}$$

and the corrected nonlinear absorption coefficient is given by:

$$\beta'(\tau_0) = \rho(\tau_0)\beta_{\mathrm{cw}}. \tag{S16}$$

In Eq. S17, we introduced the correction factor:

$$\rho(\tau_0) = \max(\bar{P}[h_\Gamma * \bar{P}]), \tag{S17}$$

which gauges the convolution by finding the peak value of $\bar{P}[h_\Gamma * \bar{P}]$, where $\bar{P}(\tau) = P(\tau)/P_0$ is the power normalized to its peak value. For the approximation in Eq. S14, we assumed that the left and right-hand sides of the equation overlap temporally. The accuracy of this approximation can be verified directly by calculating functions $P(\tau)[h_\Gamma * P](\tau)$ and $\rho(\tau_0)P^2(\tau)$ for a Gaussian pulse $P(\tau) = \exp(-\tau^2/\tau_0^2)$. Figure S3 shows functions $[h_\Gamma * P](\tau)$, $P(\tau)[h_\Gamma * P](\tau)$, and $\rho(\tau_0)P^2(\tau)$ for the pulse durations 200 fs and 3 ps. The convolution of the power and the temperature response function of gold is significantly different in these two cases. The shape of $[h_\Gamma * P](\tau)$ is similar to $h_\Gamma(\tau)$ for 200 fs pulses, while it is similar to $P(\tau)$ for 3 ps pulses. However, in both cases, the total nonlinear response of gold relevant for the nonlinear absorption dynamics $P(\tau)[h_\Gamma * P](\tau)$ is Gaussian-like in shape and very close to the shape of $P^2(\tau)$; this justifies the approximation used in Eq. S14. For comparison, Figure S3 also shows the correction factor calculated for Gaussian and sech^2-shaped $P(\tau) = \mathrm{sech}^2(\tau/\tau_0)$ pulses, which are almost identical.

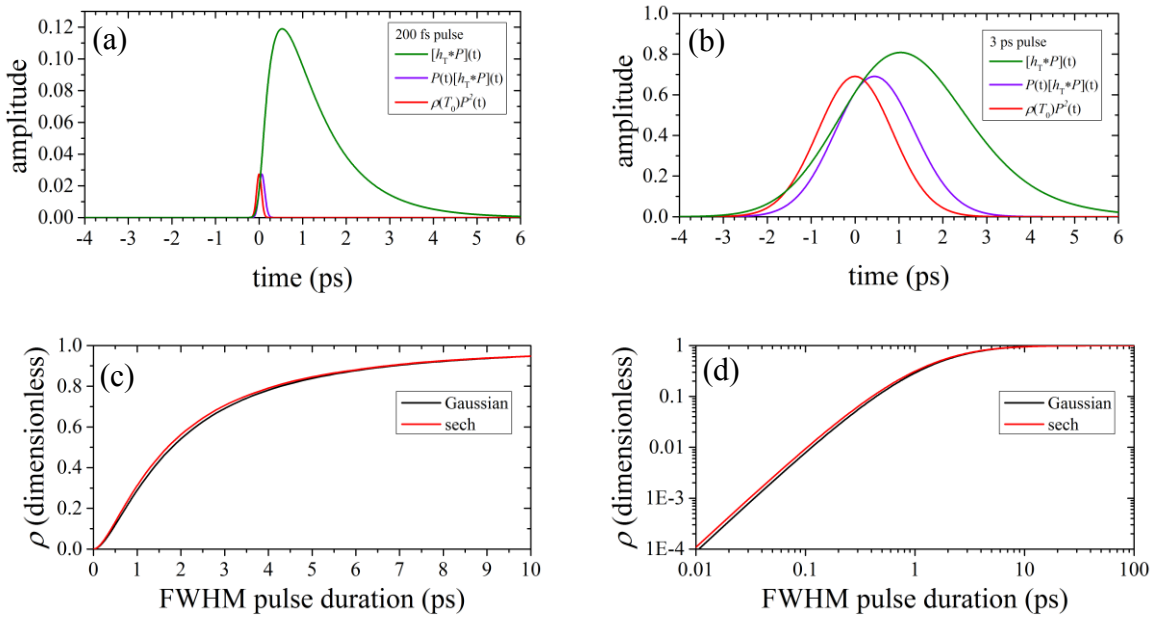

Figure S3. Validation of the approximation used in Eq. S15 for a Gaussian pulse. The convolution of the power and temperature response function $[h_T * P](\tau)$ (green), the total nonlinear term $P(\tau)[h_T * P](\tau)$ (violet), and the approximation using the correction factor $\rho(\tau_0)P^2(\tau)$ (red) for both 200 fs (a) and 3 ps (b) pulses. (c) and (d) The correction factor $\rho(\tau_0)$ for Gaussian and sech^2-shaped pulses.

We calculated the enhancement factor D for a Gaussian-shaped input pulse in the range from 10 fs to 10 ps, and we show in Figure S4 that relation $D = \rho(\tau_0)D_{cw}$ indeed holds, i.e. that the mode enhancement factors are connected to a long-pulse limit (cw) value by the correction factor $\rho(\tau_0)$. Here, we used the cw value as a free parameter. The experimental results and theoretical dependency (Figure S4, red curve) agree well for D_{cw} = 220 × 10^{-27} m^3/V^2 (accurate within 10%). This scaling of the enhancement factor was used in the derivation of the pulse duration dependence of the third-order susceptibility of gold (Eq. 3 in the paper). Further experiments for different pulse durations will enable to determine a more precise value of D_{cw}.

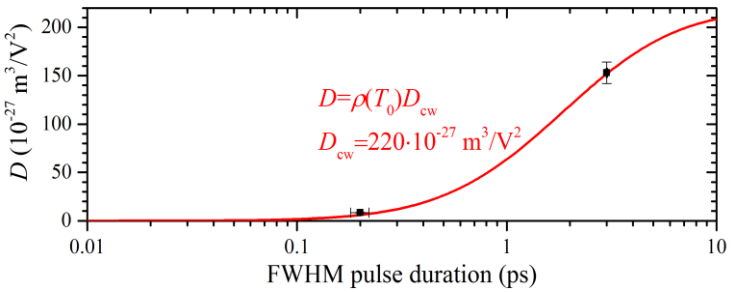

Figure S4. Pulse duration dependence of the enhancement factor D: experimental values (symbols) and model (red curve, calculated for a Gaussian pulse). The curve was calculated by $D = \rho(\tau_0)D_{cw}$, and D_{cw} was taken as a free parameter.

S5. Experimental and Theoretical Results

The experimental values of the linear propagation loss α, coupling loss C, and parameters a and β for the plasmonic waveguides with the gold layer thickness t_{Au} = 22, 27, and 35 nm are shown in Table S1. The experimental values of the imaginary part of the third-order nonlinear susceptibility $\chi^{(3)}_{Au}$ of the gold layers with the thickness t_{Au} = 22, 27, and 35 nm for 200 fs pulses at 1030 nm, and 3 ps pulses[3] at 1064 nm are presented in Table S2. The theoretical values of the third-order nonlinear susceptibility for gold layers with the thickness t = 22, 27, and 35 nm, and bulk gold for 200 fs pulses at 1030 nm are shown in Table S3.

Table S1. Experimental Values of Propagation Loss α, Coupling loss C, and Parameters a and β for Strip Plasmonic Waveguides with Different Gold Layer Thicknesses.

Thickness (nm)	α (dB/mm)	C (dB)	a	β ($W^{-1}m^{-1}$)
22	8.7 ± 0.1	6.8 ± 0.4	3.6×10^{-3}	6.2×10^{-3}
27	11.8 ± 0.2	6.9 ± 0.5	8.6×10^{-4}	5.8×10^{-3}
35	15.3 ± 0.4	7.0 ± 0.8	2.0×10^{-4}	5.1×10^{-3}

Table S2. Experimental Values of Imaginary Part of Third-Order Nonlinear Susceptibility of Gold Layers with Different Thicknesses for 200 fs Pulses at 1030 nm, and 3 ps Pulses at 1064 nm.[3]

Thickness (nm)	$\mathrm{Im}[\chi^{(3)}_{\mathrm{Au,\,200\,fs}}]$ (m^2/V^2)	$\mathrm{Im}[\chi^{(3)}_{\mathrm{Au,\,3\,ps}}]$ (m^2/V^2)
22	$(4.8 \pm 1.6) \times 10^{-19}$	$(10.5 \pm 2.1) \times 10^{-18}$
27	$(4.3 \pm 1.4) \times 10^{-19}$	$(8.2 \pm 1.5) \times 10^{-18}$
35	$(3.8 \pm 1.3) \times 10^{-19}$	$(6.5 \pm 1.4) \times 10^{-18}$

Table S3. Theoretical Values of Third-Order Nonlinear Susceptibility for Gold Layers with Different Thicknesses and Bulk Gold for 200 fs Pulses at 1030 nm.

Thickness (nm)	$\mathrm{Re}[\chi^{(3)}_{\mathrm{Au,\ 200\ fs}}]$ (m^2/V^2)	$\mathrm{Im}[\chi^{(3)}_{\mathrm{Au,\ 200\ fs}}]$ (m^2/V^2)
22	10.4×10^{-18}	4.2×10^{-19}
27	8.7×10^{-18}	3.3×10^{-19}
35	7.2×10^{-18}	2.6×10^{-19}
Bulk Gold	1.8×10^{-18}	1.9×10^{-19}

REFERENCES

(1) Hansperger, R. G. *Integrated Optics: Theory and Technology*; Springer: 2002.

(2) Charbonneau, R.; Berini, P.; Berolo, E.; Lisicka-Shrzek, E. Experimental Observation of Plasmon-Polariton Waves Supported by a Thin Metal Film of Finite Width. *Opt. Lett.* **2000**, *25*, 844-846.

(3) Lysenko, O.; Bache, M.; Lavrinenko, A. Third-Order Susceptibility of Gold for Ultrathin Layers. *Opt. Lett.* **2016**, *41*, 317-320.

(4) Marini, A.; Conforti, M.; Della Valle, G.; Lee, H. W.; Tran, Tr. X.; Chang, W.; Schmidt, M. A.; Longhi, S.; Russell, P. St. J.; Biancalana, F. Ultrafast Nonlinear Dynamics of Surface Plasmon Polaritons in Gold Nanowires due to the Intrinsic Nonlinearity of Metals. *New J. Phys.* **2013**, *15*, 013033.

(5) Conforti M.; Della Valle, G. Derivation of Third-Order Nonlinear Susceptibility of Thin Metal Films as a Delayed Optical Response. *Phys. Rev. B* **2012**, *85*, 245423.

(6) Lin, Z.; Zhigilei, L. V. Time-Resolved Diffraction Profiles and Atomic Dynamics in Short-Pulse Laser Induced Structural Transformations: Molecular Dynamics Study. *Phys. Rev. B* **2006**, *73*,184113.

(7) Sun, C.-K.; Vallée, F.; Acioli, L. H.; Ippsen, E. P.; Fujimoto, J. G. Femtosecond-Tunable Measurement of Electron Thermalization in Gold. *Phys. Rev. B* **1994**, *50*, 15337.

(8) Agrawal, G. P. *Nonlinear Fiber Optics*; Elsevier: 2013.

(9) Lysenko, O.; Bache M.; Lavrinenko, A. Nonlinear Optical Model for Strip Plasmonic Waveguides. *J. Opt. Soc. Am. B* **2016**, *33*, 1341-1348.

(10) Boyd, R. W.; Shi, Z.; De Leon, I. The Third-Order Nonlinear Optical Susceptibility of Gold. *Opt. Commun.* **2014**, *326*, 74-79.